A Refined Global Segmentation of X-ray CT Images for Multi-phase Geomaterials

Kalehiwot Nega Manahiloh[1], Kokeb A. Abera[2], and Mohammad Motalleb Nejad[3]

Abstract

X-ray computed tomography (CT) images of three-phase silica sand and glass bead specimens are analyzed and used to evaluate the segmentation performances of Otsu-, and recursion-based multilevel algorithms. A global image segmentation technique that combines iterative and recursive algorithms, namely a refined statistics-based global segmentation is proposed for segmenting multi-phase granular geomaterials. The performance of the proposed algorithm is tested by segmenting partially saturated silica sand and glass bead specimens. For the tested silica sand specimen, the refined statistics method estimated void ratio and degree of saturation were 0.67 and 39.35%. The estimates for the glass bead specimen yielded 0.64 and 43.49%, respectively. The true void ratio (0.66) and degree of saturation (37.71%) were determined with a user-controlled Image processing software package—Image-Pro. It was found that the proposed method estimated the void ratio and the degree of saturation with 1.52 and 4.35 percent errors for the silica sand and with 15.63 and 0.34 percent errors for the glass bead, respectively. The computational time of the proposed method was found to be shorter than other methods considered. Overall, it is concluded that the proposed technique performed better in segmenting three-phase granular geomaterials.

Citation information: please cite this work as follows

Link to the published material: https://link.springer.com/article/10.1007%2Fs10921-018-0508-y

---

[1] Corresponding Author, Assistant Professor, Dept. of Civil and Environmental Engineering, University of Delaware, Newark, DE 19716, email: knega@udel.edu, ORCID: 0000-0003-3568-5110.
[2] Graduate Student, Civil and Environmental Engineering, University of Delaware, Newark, DE 19716.
[3] Graduate Student, Dept. of Civil and Environmental Engineering, University of Delaware, Newark, DE 19716.

Introduction

Image segmentation is a general term applied to the techniques utilized to separate an area of interest, a pattern, or a subset of pixels with common features in an image (Liao et al. 2001). For images acquired via X-ray computed tomography (CT) scanning, each pixel contains gray-level intensity information. The intensity of each pixel can vary from black (weakest shade of gray) to white (strongest shade of gray) (Madra et al. 2014). The intensity value for each pixel is saved as an aggregate of bits. For an 8-bit image, the intensity value varies from 0 to 255. The common practice in image segmentation is to extract the pixels with the desired color or gray intensities. For images of a partially saturated granular geomaterial, three-phase segmentation aims at separating the gaseous-fluid, solid, and liquid-fluid phases, which may partially fill the pores.

Since the pioneering work of Brice and Fennema (1970), image segmentation techniques have undergone immense evolution, including in the direction of histogram thresholding. Thresholding is a simple concept that introduces one or more intensity values to an intensity distribution (i.e., image histogram) of an image where these values separate the objects of interest (i.e., foreground) from the background. Depending on the constituent elements (i.e., phases) of an image, thresholding techniques could be bi-level or multi-level (Leedham et al. 2003). Bi-level thresholding techniques introduce one threshold value to the histogram and give a two-phase segmented image (Kohler 1981; Pal and Pal 1993). Foreground and background are the terms applied to the pixel values greater than and less than the threshold value, respectively (Abdullah et al. 2012; Kurita et al. 1992). Multi-level thresholding methods, on the other hand, introduce more than one threshold value to the histogram (Arora et al. 2008; Kapur et al. 1985). Regardless of the approach, the number of segmented regions is always equal to the number of thresholds plus one.

Thresholding techniques are divided into two general classes: global and local thresholding. While global thresholding techniques use the statistical information of an intensity value distribution for the total pixels in a given image, local thresholding methods use the statistical information of a set of neighboring pixels to classify a pixel (Singh et al. 2011). The main problem associated with global thresholding techniques is that the effects of noise (i.e., random variation in pixel intensity) cannot be eliminated by these methods (Leedham et al. 2003). However, for segmentation of images with clear distinct phases, as is the case in granular materials, global thresholding techniques provide sufficiently accurate results. Numerous global thresholding techniques such as Otsu's (1979) method have been proposed by several researchers. In the presented work, the concepts of Otsu's (1979) method are employed to modify the pre-existing technique and propose a new, three-phase segmentation technique, Refined statistical-based method, for partially saturated geomaterials.

Before proceeding any further, it is important to mention that the images of this study have a relatively low resolution. Regardless, the images still have sufficient resolution that enabled the clear identification of the three phases. The authors also acknowledge that global segmentation is not the absolute ideal segmentation approach in multiphase image processing. However, this paper aims to prove a point that global segmentation techniques can be expanded upon to provide results that are equally accurate as those of other successful techniques, such as watershed segmentation and active converging contours. In addition, even though Otsu's method is not considered the state-of-the-art technique, it is considered to be a highly effective segmentation method, thus serving as a good benchmark to surpass.

Usage of global segmentation techniques prevent the need for specialty software (e.g., Volume Graphics®, Image-Pro®, and Avizo®) that may not be readily, or easily available. In

this study, a simple Gaussian filter is used for image enhancement. This filtering technique was found to handle the task satisfactorily, albeit not as precise as the more sophisticated filtering techniques such as the edge detection based anisotropic diffusion (Catte et al. 1992; Perona and Malik 1990; Sheppard et al. 2004) and nonlocal means filter (Buades et al. 2005). For this work, porosity was chosen as a benchmark parameter for evaluating segmentation performance. In reality, it may be argued that porosity is not the best choice as a benchmark parameter compared to permeability and capillary pressure. However, evaluation of such parameters requires special software programs with pre-programmed pore-morphology analyzing capabilities, that of which was neither available nor the focus of this study.

Image Acquisition

In today's market, various X-ray CT systems ranging from benchtop synchrotron microtomography to industrial X-ray image acquisition systems are available as nondestructive options for imaging granular geomaterials (De Chiffre et al. 2014). Fig. 1 shows a generalized setup of image acquisition systems. An X-ray beam, originating from an X-ray source, penetrates through a specimen seated on a pedestal with four degrees of freedom (i.e., horizontal, vertical, rotational). As the beam passes through the specimen, a projection of the specimen's internal absorption coefficients is rendered. During data acquisition, the part of the specimen through which X-ray beam passes is rendered when the pedestal completes a full 360° rotation.

An image is represented through the digitalization of a two-dimensional discrete function, f(x,y). Solving the discrete function yields a two-dimensional matrix where each element of such matrix is known as a pixel (Pal and Pal 1993). The values of x and y in a discrete function represent the row and column indices, respectively. Mathematically, image pixels form a square

or rectangular- array. In three-dimensional space, a pixel becomes a voxel (Manahiloh et al. 2012; Manahiloh et al. 2015, 2016).
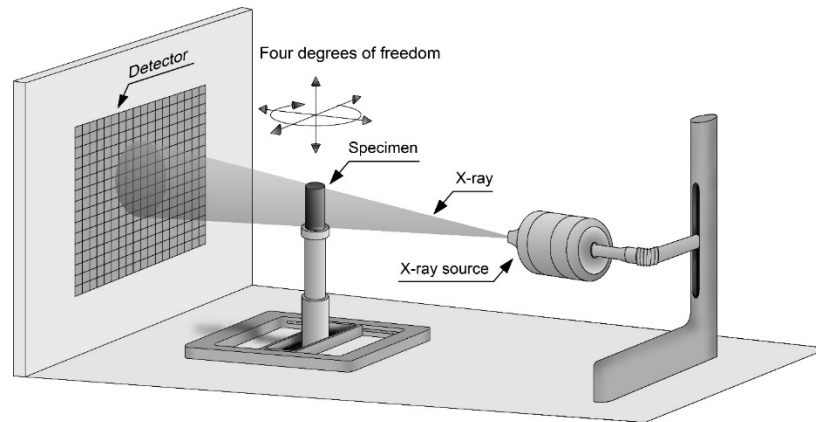
FIG. 1 General specimen installation in an X-ray CT chamber

The use of X-ray CT images and the techniques of image processing has gained interest in the geo-engineering fields. The advancements in image acquisition and processing has enabled advances in quantitative interpretations that are related, but not limited to: strain localization phenomena such as shear banding (Alshibli and Hasan 2008; Alshibli and Alramahi 2006; Alshibli et al. 2000; Masad and Somadevan 2002); distribution analysis of asphalt, soil, aggregate, and rocks microstructure (Chandan et al. 2004; Gebrenegus 2009; Ghalib and Hryciw 1999; Kim et al. 2003; Masad and Button 2000; Masad et al. 2002; Masad et al. 2002; Masad et al. 1999; Razavi 2006; Wang et al. 2004; Zelelew and Papagiannakis 2011); and multiphase porous media (Al-Raoush and Willson 2005; Al-Raoush and Willson 2005; Carminati et al. 2007; Culligan et al. 2006; Iassonov et al. 2009; Kaestner et al. 2008; Lehmann et al. 2006; Manahiloh et al. 2012; Sheppard et al. 2004; Wildenscheld et al. 2002). Almost all known quantitative analysis from image processing undergoes a very important step, namely image segmentation.

Image Segmentation

Typically, grayscale images are converted into binary images -using a manually or automatically selected threshold- to increase implementation efficiency. Binary images are segmented images in which there are only two possible values for each pixel: zero or one (Abdullah et al. 2012). In a segmented binary image, any pixels assigned a value of zero correspond to the background and pixels with a value of one correspond to the objects of interest (i.e., foreground). Compared to grayscale images, 1-bit monochrome binary images use less storage space since pixels in a binary image have two possible values rather than the 256 possible values in the case of an 8-bit grayscale image. Consequently, binary images provide faster processing speeds when thresholding algorithms are utilized (Arifin and Asano 2006).

In general, the structure for image segmentation can be viewed as a three-step process: preprocessing, segmentation algorithm application, and postprocessing (Yang and Kang 2009). When viewing an image's gray-level histogram, it may be apparent that some of the features do not form distinguishable peaks, because of noise in the image (Leedham et al. 2003). The first step, preprocessing, uses image processing tools such as a Gaussian filter (Tsai 1995) to minimize image noise that would hinder segmentation performance. In the second step, using a predetermined threshold value, the image is segmented into different, identifiable regions. Lastly, postprocessing is used to extract valuable information from portions of the segmented image, e.g., to count the number of liquid and air pixels for calculating the degree of saturation in partially saturated granular geomaterials. Postprocessing is also useful for combining unreasonably discontinuous regions in the segmentation (Yang and Kang 2009). Note that the first and third steps may not be used, because these steps depend on the quality of the original image and the effectiveness of the applied thresholding algorithm, respectively.

Implementation of Thresholding Techniques

Table 1 provides some examples of thresholding techniques that have been applied for porous media analysis since 1978. These techniques are applicable in both two-dimensional and three-dimensional image processing. As listed in the table, images of granular soils and glass bead specimens were used for validating the thresholding algorithms chosen by the authors. In an attempt to further the field of image segmentation of partially saturated granular media, this study proposes a new, three-phase image segmentation technique in which a refined statistics-based thresholding algorithm is employed.

TABLE 1 Examples of past studies for granular media thresholding

Reference	Material	Thresholding type
Ridler and Calvard (1978)	Glass beads	2D
Kurita et al. (1992)	Glass beads, sandstone	2D
Wildenschild et al. (2002)	Sand	3D
Van Geet et al. (2003)	Limestone, sandstone	3D
Vogel et al. (2005)	Sintered glass	3D
Culligan et al. (2006)	Glass beads	3D
Nunan et al. (2006)	Aggregates	2D
Carminati et al. (2007)	Soil	3D
Jassogne et al. (2007)	Soil	2D
Schaap et al. (2007)	Glass beads	3D
Kaestner et al. (2008)	Soil	3D
Lee et al. (2008)	Soil	2D
Baveye et al. (2010)	Soil	3D
Schlüter et al. (2010)	Soil	2D
Ojeda-Magaña et al. (2014)	Soil	3D

As previously indicated, the algorithms representing the modification and extensions of Otsu's (1979) method, as well as the one proposed here, were coded with MATLAB© (Mathworks 2015). Three of the techniques, Otsu's (1979) three-phase method, the iterative Otsu method, and the refined statistics-based method, were modified for proper application in MATLAB©. For coding purposes, the range of grayscale pixel intensities for the analyzed 8-bit images is 1-256, rather than 0-255.

In this study, three-phase images (solids, water, and air) of unsaturated granular

geomaterials were used. Each technique searches for two optimum threshold values, namely

threshold one (t1) and threshold two (t2). Pixels greater than t1 refer to solid particles and were

rendered with white color during segmentation. Pixels less than t2 refer to air pixels and were

rendered black during segmentation. Any pixels between t1 and t2 refer to water pixels and were

colored gray. Once a technique chose the pixel values yielding the optimal thresholds, three-

phase segmentation was performed, and the void ratio and degree of saturation were calculated

from the segmented images. Void ratio was determined by dividing the number of void pixels by

the number of solid pixels. Degree of saturation was determined by dividing the number of water

pixels by the number of void pixels, expressed as a percentage. Since the scanned images

represent a three-phase system, void pixels consist of water and air pixels.

Otsu (1979) proposed one of the oldest and most widely used global thresholding

techniques, where an optimal threshold value is selected as the pixel value located at a sharp

valley between peaks representing the objects and background of an image's gray-level

histogram (Otsu 1979). The basis of this technique separates the two classes by minimizing

within-class variance or maximizing between-class variance for optimal threshold selection. In

other words, the optimal threshold value is the pixel value that results in the minimized

summation of the foreground and background spreads (Sahoo et al. 1988).

Equations 1-4 are used for Otsu's (1979) three-phase method, where the optimal

threshold values (i.e., t1 and t2) are taken as the pixel values yielding the maximum value of

Equation 4. Note that these four equations are first applied to the entire range of pixels

represented by the gray-level histogram to obtain threshold one. Threshold two is then

determined by applying the same four equations, but this time to a refined histogram ranging

from the smallest pixel value to the value of threshold one.

$$mean = \frac{\sum\limits_{i=1}^{m} i * f_i}{m} \tag{1}$$

$$meanli = \frac{\sum\limits_{i=1}^{t-1} i * f_i}{m} \tag{2}$$

$$meangi = \frac{\sum\limits_{i=t}^{m} i * f_i}{m} \tag{3}$$

$$t = \arg\max\{\sum\limits_{i=1}^{t-1} f_i * \{meanli - mean\}^2 + \sum\limits_{i=t}^{m} f_i * \{meangi - mean\}^2\} \tag{4}$$

In the above equations, m is the highest possible pixel value in an image (here, since 8-bit

images are processed in MATLAB, the highest possible value is 256); i represents a pixel value

within the range of one to m; f represents the individual pixel frequencies; mean, meanli, and

meangi represent the mean of an image's pixel intensities ranging from one to m, one to t-1, and t

to m, respectively; t refers to the optimal threshold value of either t1 or t2.

As with the previous method, the iterative Otsu method calculates threshold one (t1) with

Equations 1-4. The initial value for threshold two (t2) is calculated with Equations 5-7. The

reason for expanding Otsu's (1979) three-phase method into the iterative Otsu method is because

the procedure followed for finding the threshold two value through Otsu's (1979) three-phase

method does not necessarily result in the optimal value. The usage of Equations 8-10 determines

a threshold value referred to as threshold new (tnew). Equations 8-10 are then used again in a

loop (threshold new is assigned as threshold two) and the loop terminates once the value of

threshold new is within two gray-level pixel values of the previous iteration. Once this criterion

is met, the threshold new values will be assigned as the optimal value of threshold two.

$$mean1 = \frac{\sum_{i=1}^{t1} i * f_i}{\sum_{i=1}^{t1} f_i} \tag{5}$$

$$mean2 = \frac{\sum_{i=t1+1}^{m} i * f_i}{\sum_{i=t1+1}^{m} f_i} \tag{6}$$

$$t2 = \frac{(mean1 + mean2)}{2} \tag{7}$$

$$mean3 = \frac{\sum_{i=1}^{t2} i * f_i}{\sum_{i=1}^{t2} f_i} \tag{8}$$

$$mean4 = \frac{\sum_{i=t2+1}^{m} i * f_i}{\sum_{i=t2+1}^{m} f_i} \tag{9}$$

$$tnew/t2 = \frac{(mean3 + mean4)}{2} \tag{10}$$

Equations 11-12 represent the refined statistics-based method where the optimal values

for threshold one and two are determined for extracting three phases of a partially saturated

granular media by assuming that the thresholding values are located within unknown numbers of

standard deviation from the left and right of the mean pixel intensity values. This proposed

method follows the concept that numerous distributions have a tendency to follow the Dirac delta

function with the peak located near the mean pixel intensity values (Arora et al. 2008). The mean

(μ) and standard deviation (σ) of the frequencies of all of the pixels in the image are determined.

As mentioned in the work of Arora et al. (2008), many images contain normally distributed

histograms. An estimation of such a histogram is a Gaussian distribution. Such histograms have

high frequency values concentrated around a certain value (i.e., the mean pixel intensity value).

Also, on a visual standpoint, it is much easier to distinguish objects from the background at

intensity values near the mean. However, not all images have histograms with normal

distributions. Fitting parameters, k1 and k2, are then utilized to provide effectively segmented

images with asymmetric or skewed histograms. Through alteration of the fitting parameters, the

concepts applied for normally distributed histograms adapt to non-uniform distributions.

Arora et al. (2008) provides similar equations to those in Equations 11-12. However, the methodology of that work tries to find two or more thresholding values to represent an image with multiple shades of intensity. Here, the three different phases of partially saturated granular geomaterials are to be accurately captured, which implies the usage of two thresholding values and imposes a trial-and-error approach. Arora et al. (2008) chose a value of one for both k1 and k2 for simplicity. The images used in that study were random (e.g., woman, peppers, jet, house). The proposed method does not provide successful segmented images for the geomaterials of this study when the values of k1 and k2 are equal to one. By adjusting these parameters, it is seen that the method is more sensitive to the value of k1 than the value of k2. A trial-and-error process was implemented to search for k1 and k2 values to obtain a segmented image that effectively captures all of the portions of the raw image. For the geomaterials used in this study, it is recommended that k1 range from zero to two and that k2 range from zero to three, while ensuring that k2 is always greater than k1. These conditions for the fitting parameters vary depending on the type of images being analyzed. Overall, the proposed method provides a faster processing time than both the Arora et al. (2008) method and Otsu's (1979) three-phase method and superior thresholding values compared to Otsu's (1979) three-phase method.

The proposed method utilizes modified-statistical information, in comparison to the Arora et al. 2008, to provide higher-quality segmented images and faster processing time. The key difference in the image segmentation step between these two methods is that the Arora et al. 2008 method was tested on generic images whereas the proposed method was specifically created for analyzing various geomaterials. As previously mentioned, the algorithm proposed by Arora et al. (2008) is capable of finding multiple thresholding values (as many as the user desires) to apply for image segmentation. However, in the presented work, it is specifically

shown that modifying the Arora et al. (2008) algorithm leads to more reliable thresholds for three-phase geomaterials. In contrast to the Arora et al. (2008) method, a sensitivity analysis was conducted on the images of the geomaterials used in this study to recommend a range of values for the fitting parameters, k1 and k2. Adding restrictions to these values can significantly reduce processing time, lead to more accurate threshold selection, and improve segmentation.

$$t1 = abs\left(\mu + \frac{\sigma * (k2 - k1)}{2}\right) \tag{11}$$

$$t2 = abs\left(\frac{\sigma * (k1 + k2)}{2}\right) \tag{12}$$

Results and Discussion

The three thresholding techniques described in the preceding section were applied to X-ray CT images obtained for two different partially saturated specimens made out of silica sand and glass beads. For presentation purposes, and for comparison of the performance of each thresholding technique, the first image slice of the image set for each specimen was used.

A standalone executable software program, with a graphical user interface (GUI) and embedment of the aforementioned techniques, was developed and used to run image analyses. In addition to its user-friendly environment, this application was packaged in a way so that MATLAB© software would not be required to perform the analyses. Before segmenting an image, it is necessary to ensure the raw images are cropped into an exact area-of-interest (AOI). For the images analyzed here, since the cross-sectional area of the scanned specimens was circular, all images needed to be cropped using a circular AOI window. That way, pixels that were not in the AOI would not be included in the statistical analysis. Otherwise, the calculated values for void ratio and degree of saturation would suffer from significant errors.

Codes can be written to perform either automatic or manual cropping. Automatic cropping has proven to be undependable, due to being greatly affected by the conditions in which a specimen is scanned and how the scanned images are rendered. For example, an X-ray CT system may include a specimen's container during scanning, and a scale representing particle sizes might be placed on image slice renderings. Automatic cropping procedures attempt to locate the boundaries of a specimen based on pixel information and will incorrectly assume that the cropped boundaries include portions of the container and the scale. This occurrence also holds true if the specimen is not centered during imaging. The standalone software allows users to draw the cropping window on top of the opened X-ray image and save it. The same crop window can then be used to crop all of the remaining images.

The silica sand specimen had an original and cropped diameter of 6.35 mm and was newly prepared in a laboratory setting. Ninety image slices were obtained for this specimen through X-ray CT scanning. In order to quantitatively verify the accuracy of the results of the three techniques, the void ratio and degree of saturation for this specimen were also determined with the image processing software, Image-Pro© (Image-Pro Plus). These values were found to be 0.66 and 37.71%, respectively. Fig. 2 shows the first silica sand image slice with the applied manual crop as displayed in the standalone software developed as part of this study.
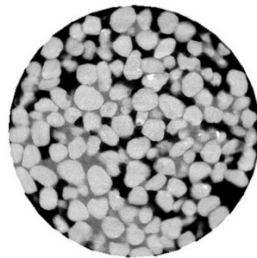
FIG. 2 First cropped image slice of a partially saturated silica sand specimen
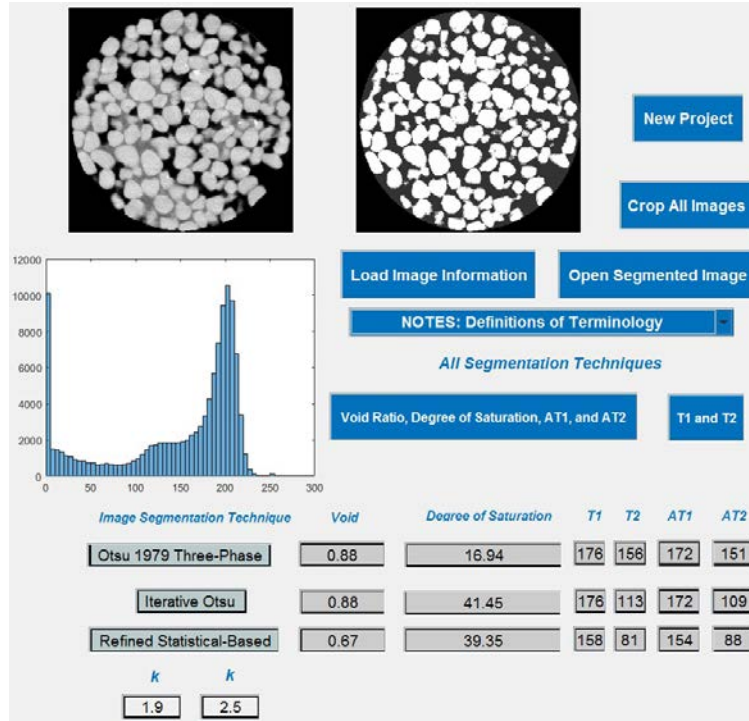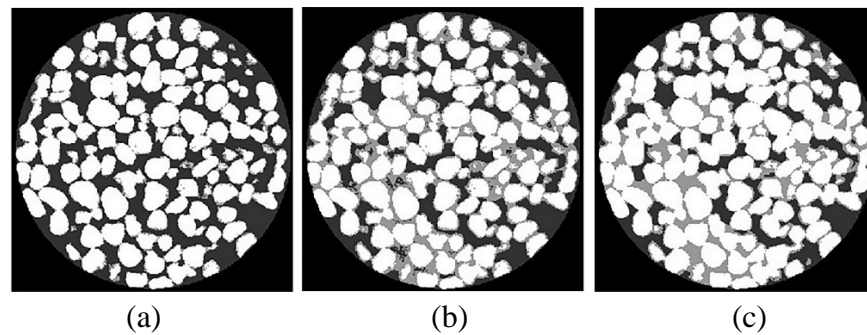
FIG. 3 Partially saturated silica sand results of thresholding techniques (Displayed image slice segmented with Otsu's (1979) three-phase method)

Fig. 3 represents the quantitative results from the applied thresholding techniques. The void ratio and degree of saturation of the specimen, and average values of threshold one and threshold two for the techniques are displayed in the figure. The values of threshold one and threshold two for the first image slice are also provided for each technique. The raw and segmented X-ray CT images of the first slice are displayed together with its corresponding gray-level histogram. In this specific case, Otsu's (1979) three-phase segmentation technique was applied. Fig. 4 presents the segmented images for the same image slice when different thresholding methods were applied.

Fig. 4 shows that Otsu's (1979) three-phase method, the iterative Otsu method, and the refined statistics-based method calculated void ratios of 0.88, 0.88, and 0.67, respectively. The two Otsu-based methods produced the same average threshold one value of 172. In this context, "average" refers to the average of threshold values calculated for all images in the set. As a

result, Otsu's (1979) three-phase method and the iterative Otsu method yielded the same number of solid pixels, thus explaining the same void ratio value between these methods. The three methods had average threshold two values of 151, 109, and 88, respectively. The value for the degree of saturation varied with threshold two due to the degree of saturation being a relationship between water and void pixels. Specifically for the Otsu-based methods, due to the number of solid pixels remaining the same, a lower threshold two value resulted in a higher degree of saturation and vice versa. The degrees of saturation for Otsu's (1979) three-phase method and the iterative Otsu method were determined as 16.94% and 41.45%, respectively. Quantitatively, these methods overestimated void ratio. This led to the solid particles in Figs. 4a and 4b being slightly too eroded. Otsu's (1979) three-phase method greatly underestimated the degree of saturation with more than 50% error, as compared to the degree of saturation obtained from Image-Pro© (visible in Fig. 5a). The iterative Otsu method slightly overestimated the degree of saturation, compared to Image-Pro, by approximately 10%. However, as observed in Fig. 4b, the segmented silica sand specimen has portions containing water not appearing in the original image slice or portions lacking water and thus containing more voids.

(a)   (b)   (c)

FIG 4 Segmented images of a partially saturated silica sand slice: (a) Otsu's (1979) three-phase method, (b) iterative Otsu method, (c) refined statistics-based method

On average, the refined statistics-based method had the smallest threshold two value and a degree of saturation value of 39.35%. The k1 and k2 parameters for this method were chosen

15

as 1.9 and 2.5, respectively. A trial-and-error process was utilized to obtain parameters that

resulted in segmented images which effectively captured the three phases of the raw images. For

this method, the average value of threshold one was found to be 158, indicating that more solid

pixels and fewer void spaces were captured in the segmentation. By comparing the results of

Figs. 4a-4c, it is apparent that Fig. 4c accurately contains more bridges of water between the

solid particles and fewer voids within the solid particles, as seen in the original slice (Fig. 2).

Quantitatively, the void ratio and degree of saturation results of the proposed method are very

accurate to the results of Image-Pro, with approximately 1.52% and 4.35% error, respectively.

The effectiveness of the proposed method was tested against the Arora et al. (2008) method

while qualitatively keeping the segmentations the same (Fig. 5). Note that the values of k1 and

k2 differ between the methods since the role of these parameters in the algorithms are not the

same. The proposed method was found to have significantly faster processing time than both the

method of Arora et al. (2008) and Otsu's (1979) three-phase method, as shown in Table 2. For

these reasons, the proposed method proved to be superior to the Arora et al. (2008) method. In

conclusion, the segmentation of the silica sand specimen was best captured by the refined

statistics-based method, both qualitatively and quantitatively.

(a)   (b)
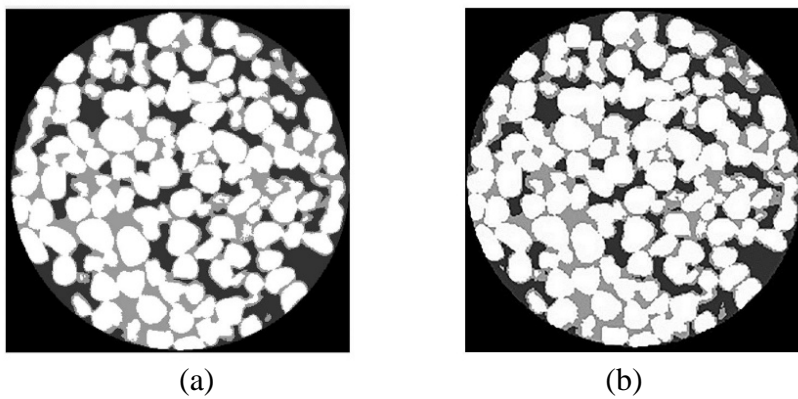
FIG. 5 Segmented images of a partially saturated silica sand slice: (a) Arora et al. (2008)
method, (b) refined statistics-based method

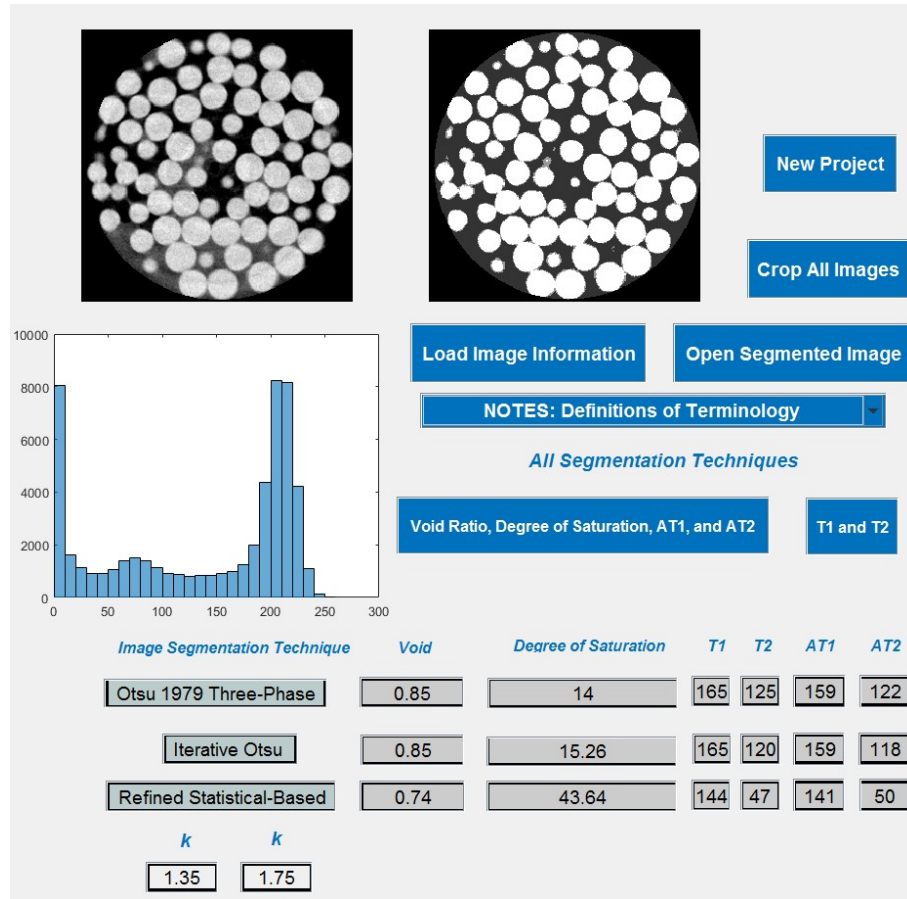**TABLE 2** Processing time comparison for the silica sand specimen

Method	Processing time (s)	Percent decrease Arora et al. (2008) to refined statistics-based)	Percent decrease Otsu (1979) to refined statistics-based)
Arora et al. (2008) (k1=0.62, k2=3.85)	5.79		
Otsu (1979) three-phase	5.89	70.12%	70.63%
Refined statistics-based (k1=1.9, k2=2.5)	1.73		

The glass bead specimen had an original and cropped diameter of 10 mm; ninety image slices, the first of which is depicted in Fig. 6, were obtained for this specimen through X-ray CT scanning, as with the silica sand specimen. Fig. 7 provides the quantitative results of the applied thresholding techniques (first image slice used for calculating t1) and the segmentation of the first image slice with Otsu's (1979) three-phase method applied. Lastly, Fig. 8 presents the segmentation of the first glass bead image slice per thresholding technique. The Image-Pro void ratio and degree of saturation values were found to be 0.64 and 43.49%, respectively.

Following the same algorithmic trend as observed with the results of the silica sand specimen, Otsu's (1979) three-phase method and the iterative Otsu method yielded the same void ratio of 0.85 and average threshold one value of 159. Respectively, the degrees of saturation were 14% and 15.26%. By analyzing Figs. 8a-8b, the segmentations failed to capture the majority of the water pixels seen in the original slice. This is due to the methods determining threshold two values that were too high. A higher threshold two-value results in a segmented image containing fewer water pixels and more air pixels, thus providing a lower degree of saturation.
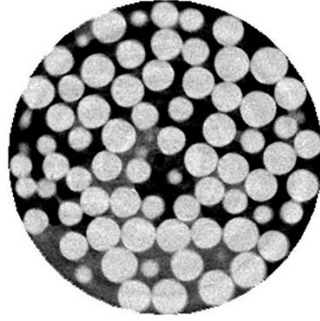
FIG. 6 First cropped image slice of a partially saturated glass bead specimen

Image Segmentation Technique	Void	Degree of Saturation	T1	T2	AT1	AT2
Otsu 1979 Three-Phase	0.85	14	165	125	159	122
Iterative Otsu	0.85	15.26	165	120	159	118
Refined Statistical-Based	0.74	43.64	144	47	141	50

k 1.35   *k* 1.75

FIG. 7 Partially saturated glass bead results of thresholding techniques (Displayed image slice segmented with Otsu's (1979) three-phase method)
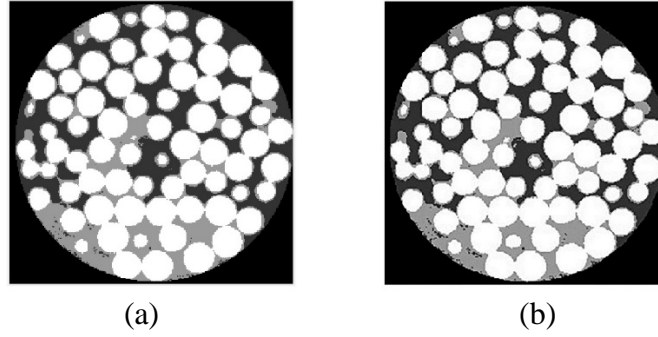

(a)　　　　　　　(b)　　　　　　　(c)
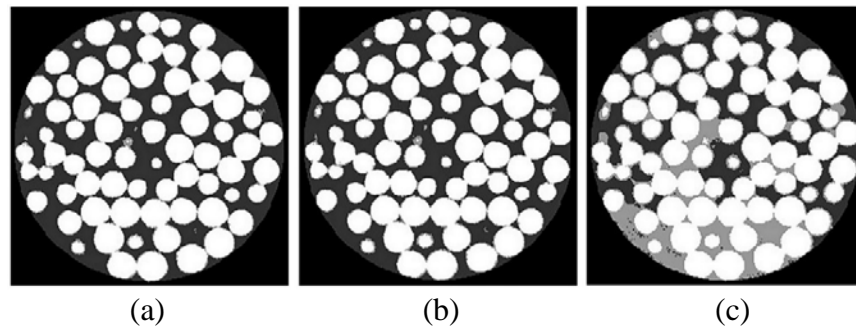
FIG. 8 Segmented images of a partially saturated glass bead slice: (a) Otsu's (1979) three-phase method, (b) iterative Otsu method, (c) refined statistics-based method

Even though the iterative Otsu method did a slightly better job at capturing the water pixels than Otsu's (1979) three-phase method, the degree of saturation was still approximately three times smaller than the Image-Pro value. The void ratio and degree of saturation for the refined statistics-based method, with k1=1.35 and k2=1.75, were 0.74 and 43.64%, respectively. For this method, the average values of threshold one and threshold two were 141 and 50, respectively. The proposed method's average threshold two value is more than two times smaller than those of the two techniques based on Otsu (1979). This decrease led to significantly more water pixels being captured, as visible in Fig. 8c. Quantitatively, the degree of saturation of the proposed method was very accurately determined, in comparison to the Image-Pro value, with approximately 0.34% error. As with the silica sand specimen, the superiority of the refined statistics-based method to the Arora et al. (2008) method was evaluated. Once again, the processing time for the proposed method was much faster (Table 3) with the segmentation of the glass bead specimen remaining the same between the Arora et al. (2008) and proposed methods (Fig. 9). Overall, the segmentation of the glass bead specimen was best captured by the refined statistics-based method.

TABLE 3 Processing time comparison for the glass bead specimen

Method	Processing time (s)	Time reduction by Refined-statistics from:	
		Arora et al. (2008)	Otsu (1979)
Arora et al. (2008) (k1=0.19, k2=4.55)	6.21	84.54%	80.49%
Otsu (1979) three-phase	4.92		
Refined statistics-based (k1=1.35, k2=1.75)	0.96		

(a)   (b)

FIG. 9 Segmented images of a partially saturated glass bead slice: (a) Arora et al. (2008) method, (b) refined statistics-based method.

Table 4 lists the final results of the refined statistics-based method for the partially saturated granular media. Tables 5-8 provide statistical results for the three methods applied to each geomaterial. The proposed method's results for the silica sand specimen showed that there were moderately low percent errors of 1.52 and 4.35 for void ratio and degree of saturation, respectively, in comparison to the values provided by Image-Pro. Interestingly, the results of the glass bead specimen showed that the percent error associated with void ratio was a high 15.63 and the percent error associated with the degree of saturation was a very low 0.34.

As indicated previously, threshold one separated solid pixels from water and air pixels and threshold two separated water pixels from air pixels. The percent errors for the silica sand specimen suggested that the fitting parameters, k1 and k2, for the refined statistics-based method had a greater influence on threshold two and had a low effect on threshold one. On the other hand, the chosen fitting parameters for the glass bead specimen had a great influence on threshold one and not so much on threshold two.

These findings led to the hypothesis that the proposed refined statistics-based method was more accurate at determining one geomaterial property rather than multiple properties (e.g., void ratio and degree of saturation). More images of partially saturated granular media would have to be analyzed to test the validity of this hypothesis. Regardless, the freedom and flexibility of

choosing fitting parameters proved this method's superiority to the other two Otsu-based methods. Being able to apply a range of fitting parameters allows the proposed method to be adaptable to a wide range of images.

TABLE 4. Refined statistics-based method results for the partially saturated granular media

Granular media	Segmentation technique	Void ratio	Degree of saturation	% error (void ratio)	% error (degree of saturation)
Silica sand	Refined-statistics (k1=1.9, k2=2.5)	0.67	39.35%	1.52%	4.35%
Glass bead	Refined-statistics (k1=1.35, k2=1.75)	0.74	43.64%	15.63%	0.34%

TABLE 5. Void ratio statistical results and comparisons for the silica sand specimen

Geomaterial	Segmentation technique	Void ratio	Error	Standard deviation	Coefficient of variation (CV)
Silica sand	Otsu's (1979)	0.88	0.045		
	Iterative Otsu	0.88	0.045		
	Refined-statistics (k1=1.9, k2=2.5)	0.67	0.0001	0.099	12.22%
	Image-Pro	0.66	0.000		

TABLE 6. Void ratio statistical results and comparisons for the glass bead specimen

Geomaterial	Segmentation technique	Void ratio	Error	Standard deviation	Coefficient of variation (CV)
Glass bead	Otsu's (1979)	0.85	0.044		
	Iterative Otsu	0.85	0.044		
	Refined-statistics (k1=1.35, k2=1.75)	0.74	0.01	0.052	6.38%
	Image-Pro	0.64	0.000		

TABLE 7. Degree of saturation statistical results and comparisons for the silica sand specimen

Geomaterial	Segmentation technique	Degree of saturation	Error	Standard deviation	Coefficient of variation (CV)
Silica sand	Otsu's (1979)	16.94%	0.043		
	Iterative Otsu	41.45%	0.0014		
	Refined-statistics (k1=1.9, k2=2.5)	39.35%	0.00027	0.11	34.05%
	Image-Pro	37.71%	0.000		

TABLE 8. Degree of saturation statistical results and comparisons for the glass bead specimen

Geomaterial	Segmentation technique	Degree of saturation	Error	Standard deviation	Coefficient of variation (CV)
	Otsu's (1979)	14.00%	0.087		
	Iterative Otsu	15.26%	0.080		
Glass bead	Refined-statistics (k1=1.35, k2=1.75)	43.64%	0.000	0.14	56.32%
	Image-Pro	43.49%	0.000		

Conclusions

A refined statistics-based method was proposed and used for effective segmentation of three-phase images of partially saturated granular geomaterials. Two other methods, namely the Otsu's (1979) three-phase and the iterative Otsu, were utilized to test the performance of the proposed algorithm. Since these three techniques dealt with three-phase (solids, water, and air) image segmentation, two threshold values, *threshold one* and *threshold two*, were required for proper image segmentation. Therefore, pixels greater than threshold one were solid pixels, any pixels less than threshold two were air pixels, and all other pixels between the two threshold values were water pixels. The algorithms for the three thresholding techniques were coded into MATLAB© to ultimately determine index properties of the analyzed media, such as void ratio and degree of saturation.

Otsu's (1979) three-phase method was first evaluated as a thresholding option because it is one of the oldest, simplest, and most successful methods for determining automatic threshold values for different image types. An optimal threshold value was found by minimizing the within-class variance of the foreground and background classes of an image's gray-level histogram. For the two geomaterials analyzed, this method yielded reasonable threshold one values but not so much for threshold two. Hence, the iterative Otsu method stemmed from Otsu's (1979) three-phase method in an attempt to more accurately calculate threshold two. The

algorithm's loop terminated once the threshold value was within two gray-level pixels of the previous iteration.

Since the proposed method is a refinement of the Arora et al. (2008) method, the proposed method was found to require shorter processing time without diminishing segmentation quality. The percent errors associated with the silica sand specimen showed that segmentation results were more heavily influenced by threshold two than threshold one. The reverse was found to be true for the glass bead specimen. These findings suggested that the proposed method was more accurate at determining one geomaterial property rather than multiple properties.

The refined statistics-based method proved to be a very successful technique for image segmentation. The technique allowed user input to adapt the algorithm to be more suitable for the image of focus. The freedom and flexibility of this algorithm confirmed the superiority of the proposed method to the techniques based on Otsu (1979). The conclusions about the proposed technique could very well contribute to advancements in the field of three-phase image segmentation of granular media in the near future.

Acknowledgments

References

Abdullah, S. L. S., Hambali, H. A., and Jamil, N. (2012). "Segmentation of Natural Images Using an Improved Thresholding-Based Technique." *Procedia Engineering*, 41, 938-944.

Al-Raoush, R. I., and Willson, C. S. (2005). "Extraction of physically realistic pore network properties from three-dimensional synchrotron X-ray microtomography images of unconsolidated porous media systems." *Journal of Hydrology*, 300(1–4), 44-64.

Al-Raoush, R. I., and Willson, C. S. (2005). "A pore-scale investigation of a multi-porous media system." *Journal of Contaminant Hydrology*, 77, 67-89.

Alshibli, K., and Hasan, A. (2008). "Spatial variation of void ratio and shear band thickness in sand using X-ray computed tomography." *Geotechnique*, 58(4), 249-257.

Alshibli, K. A., and Alramahi, B. A. (2006). "Microscopic evaluation of strain distribution in granular materials during shear." *J Geotech Geoenviron Eng*, 132(1), 80-91.

Alshibli, K. A., Sture, S., Costes, N. C., Frank, M. L., Lankton, M. R., Batiste, S. N., and Swanson, R. A. (2000). "Assessment of localized deformation in sand using x-ray computed tomography." *Geotechnical Testing Journal*, 23(3), 274-299.

Arifin, A. Z., and Asano, A. (2006). "Image segmentation by histogram thresholding using hierarchical cluster analysis." *Pattern Recognition Letters*, 27(13), 1515-1521.

Arora, S., Acharya, J., Vermac, A., and Panigrahi, P. K. (2008). "Multilevel thresholding for image segmentation through a fast statistical recursive algorithm." *Pattern Recognition Letters*, 29(2), 119-125.

Baveye, P. C., Laba, M., Otten, W., Bouckaert, L., Dello Sterpaio, P., Goswami, R. R., Grinev, D., Houston, A., Hu, Y., Liu, J., Mooney, S., Pajor, R., Sleutel, S., Tarquis, A., Wang, W., Wei, Q., and Sezgin, M. (2010). "Observer-dependent variability of the thresholding step in the quantitative analysis of soil images and X-ray microtomography data." *Geoderma*, 157(1–2), 51-63.

Brice, C., and Fennema, C. (1970). "Scene analysis using regions." *Artificial Intelligence*, 1(3), 205-226.

Buades, A., Coll, B., and Morel, J. "Non-local algorithm for image denoising." *Proc., IEEE CVPR, 2005*.

Carminati, A., Kaestner, A., Hassanein, R., Ippisch, O., Vontobel, P., and Flühler, H. (2007). "Infiltration through series of soil aggregates: Neutron radiography and modeling." *Advances in Water Resources*, 30(5), 1168-1178.

Catte, F., Lions, P., Morel, J., and Coll, T. (1992). "Image selective and edge detection by nonlinear diffusion." *SIAM J. Numer. Anal.*, 29(1), 182-193.

Chandan, C., Sivakumar, K., Masad, E., and Fletcher, T. (2004). "Application of imaging techniques to geometry analysis of aggregate particles." *Journal of Computing in Civil Engineering*, 18(1), 75-82.

Culligan, K. A., Wildenschild, D., Christensen, B. S. B., Gray, W. G., and Rivers, M. L. (2006). "Pore-scale characteristics of multiphase flow in porous media: A synchrotron-based CMT comparison of air-water and oil-water experiments." *Adv. Water Resour*, 29, 227-238.

De Chiffre, L. S., Carmignato, S., Kruthc, J.-P., Schmittd, R., and Weckenmann, A. (2014). "Industrial applications of computed tomography." *CIRP Annals-Manufacturing Technology*, 63(2), 655-677.

Gebrenegus, T. (2009). "Application of X-ray Computed Tomography to Study Initiation and Evolution of Surface Cracks in Sand-Bentonite Mixtures." Ph.D., University of Idaho, Moscow.

Ghalib, A. M., and Hryciw, R. D. (1999). "Soil Particle Size Distribution by Mosaic Imaging and Watershed Analysis." *Journal of Computing in Civil Engineering*, 13(2), 80-87.

Iassonov, P., Gebrenegus, T., and Tuller, M. (2009). "Segmentation of X-ray computed tomography images of porous materials: A crucial step for characterization and quantitative analysis of pore structures." *Water Resources Research*, 45(9), 1-12.

Image-Pro Plus. [Computer software]. Version 5, Media Cybernetics, Silver Spring, MD.

Jassogne, L., McNeill, A., and Chittleborough, D. (2007). "3D-visualization and analysis of macro- and meso-porosity of the upper horizons of a sodic, texture-contrast soil." *European Journal of Soil Science*, 58(3), 589-598.

Kaestner, A., Lehmann, E., and Stampanoni, M. (2008). "Imaging and image processing in porous media research." *Advances in Water Resources*, 31(9), 1174-1187.

Kapur, J. N., Sahoo, P. K., and Wong, A. K. C. (1985). "A New Method for Gray-Level Picture Thresholding Using the Entropy of the Histogram." *Computer Vision, Graphics, and Image Processing*, 29, 273-285.

Kim, H., Haas, C. T., Rauch, A. F., and Browne, C. (2003). "3D Image Segmentation of Aggregates from Laser Profiling." *Computer-Aided Civil and Infrastructure Engineering*, 18(4), 254-263.

Kohler, R. (1981). "A segmentation system based on thresholding." *Computer Graphics and Image Processing*, 15(4), 319-338.

Kurita, T., Otsu, N., and Abdelmalek, N. (1992). "Maximum Likelihood Thresholding Based on Population Mixture Models." *Pattern Recognition*, 25(10), 1231-1240.

Lee, S. S., Gantzer, C. J., Thompson, A. L., Anderson, S. H., and Ketcham, R. A. (2008). "Using High-Resolution Computed Tomography Analysis To Characterize Soil-Surface Seals." *Soil Science Society of America Journal*, 72(5), 1478-1485.

Leedham, G., Yan, C., Takru, K., Joie, and Mian, L. "Comparison of some thresholding algorithms for text/background segmentation in difficult document images." 859-864.

Lehmann, P., Wyss, P., Flisch, A., Lehmann, E., Vontobel, P., Krafczyk, M., Kaestner, A., Beckmann, F., Gygi, A., and Flühler, H. (2006). "Tomographical Imaging and Mathematical Description of Porous Media Used for the Prediction of Fluid Distribution." *Vadose Zone Journal*, 5(1), 80-97.

Liao, P. S., Chen, T. S., and Chung, P. C. (2001). "A Fast Algorithm for Multilevel Thresholding." *Journal of Information Science and Engineering*, 17, 713-727.

Madra, A., Hajj, N. E., and Benzeggagh, M. (2014). "X-ray microtomography applications for quantitative and qualitative analysis of porosity in woven glass fiber reinforced thermoplastic." *Composites Science and Technology*, 95, 50-58.

Manahiloh, K. N., Muhunthan, B., Kayhanian, M., and Gebremariam, S. Y. (2012). "X-Ray Computed Tomography and Nondestructive Evaluation of Clogging in Porous Concrete Field Samples." *Journal of Materials in Civil Engineering*, 24(8), 1103-1109.

Manahiloh, K. N., Muhunthan, B., and Likos, W. J. (2015). "Effective stress and the role of liquid fabric in unsaturated granular soils." *Geomechanics from Micro to Macro, Vols I and II*, 863-868.

Manahiloh, K. N., Muhunthan, B., and Likos, W. J. (2016). "Microstructure-Based Effective Stress Formulation for Unsaturated Granular Soils." *International Journal of Geomechanics*, 16(6), DOI: 10.1061/(ASCE)GM.1943-5622.0000617.

Masad, E., and Button, J. W. (2000). "Unified Imaging Approach for Measuring Aggregate Angularity and Texture." *Computer-Aided Civil and Infrastructure Engineering*, 15(4), 273-280.

Masad, E., Jandhyala, V. K., Dasgupta, N., Somadevan, N., and Shashidhar, N. (2002). "Characterization of air void distribution in asphalt mixes using x-ray computed tomography." *Journal of Materials in Civil Engineering*, 14(2), 122-129.

Masad, E., Muhunthan, B., and Crowe, C. (2002). "Numerical modelling of fluid flow in microscopic images of granular materials." *Int J Numer Anal Met*, 26(1), 53-74.

Masad, E., Muhunthan, B., Shashidhar, N., and Harman, T. (1999). "Internal Structure Characterization of Asphalt Concrete Using Image Analysis." *Journal of Computing in Civil Engineering*, 13(2), 88-95.

Masad, E., and Somadevan, N. (2002). "Microstructural finite-element analysis of influence of localized strain distribution on asphalt mix properties." *J Eng Mech-Asce*, 128(10), 1105-1114.

Mathworks. 2015. Matlab 2015,Mathworks Inc., Natick, MA.

Nunan, N., Ritz, K., Rivers, M., Feeney, D. S., and Young, I. M. (2006). "Investigating microbial micro-habitat structure using X-ray computed tomography." *Geoderma*, 133(3–4), 398-407.

Ojeda-Magaña, B., Quintanilla-Domínguez, J., Ruelas, R., Tarquis, A. M., Gómez-Barba, L., and Andina, D. (2014). "Identification of pore spaces in 3D CT soil images using PFCM partitional clustering." *Geoderma*, 217–218, 90-101.

Otsu, N. (1979). "Threshold Selection Method from Gray-Level Histograms." *IEEE Trans. Syst., Man Cybernetics*, SMC-9(1), 62-66.

Pal, N. R., and Pal, S. K. (1993). "A review on image segmentation techniques." *Pattern Recognition*, 26(9), 1277-1294.

Perona, P., and Malik, J. (1990). "Scale-space and edge detection using anisotropic diffusion." *IEEE Trans. Pattern Anal. Mach. Intel.*, 12(7), 629-639.

Razavi, M. R. (2006). "Characterization of Microstructure and Internal Displacement Field of Sand using X-ray Computed Tomography." Ph.D., Washington State University, Pullman.

Ridler, T. W., and Calvard, S. (1978). "Picture Thresholding Using an Iterative Selection Method." *IEEE Transactions on Systems, Man, and Cybernetics*, 8(8), 630-632.

Sahoo, P. K., Soltani, S., and Wong, A. K. C. (1988). "A survey of thresholding techniques." *Computer Vision, Graphics, and Image Processing*, 41(2), 233-260.

Schaap, M. G., Porter, M. L., Christensen, B. S. B., and Wildenschild, D. (2007). "Comparison of pressure-saturation characteristics derived from computed tomography and lattice Boltzmann simulations." *Water Resources Research*, 43(12), 1-12.

Schlüter, S., Weller, U., and Vogel, H.-J. (2010). "Segmentation of X-ray microtomography images of soil using gradient masks." *Computers & Geosciences*, 36(10), 1246-1251.

Sheppard, A. P., Sok, R. M., and Averdunk, H. (2004). "Techniques for image enhancement and segmentation of tomographic images of porous materials." *Physica A: Statistical Mechanics and its Applications*, 339(1), 145-151.

Singh, T. R., Roy, S., Singh, O. I., Sinam, T., and Singh, K. M. (2011). "A new local adaptive Thresholding technique in Binarization." *International Journal of Computer Science Issues*, 8(2), 271-277.

Tsai, D. M. (1995). "A fast thresholding selection procedure for multimodal and unimodal histograms." *Pattern Recognition Letters*, 16, 653-666.

Van Geet, M., Lagrou, D., and Swennen, R. "Porosity measurements of sedimentary rocks by means of microfocus X-ray computed tomography (μCT)." *Proc., Applications of X-ray computed tomography in the geosciences*, Geological Society, Special publications, 51-60.

Vogel, H.-J., Tölke, J., Schulz, V. P., Krafczyk, M., and Roth, K. (2005). "Comparison of a Lattice-Boltzmann Model, a Full-Morphology Model, and a Pore Network Model for Determining Capillary Pressure-Saturation Relationships." *Vadose Zone Journal*, 4(2), 380-388.

Wang, L. B., Frost, J. D., and Lai, J. S. (2004). "Three-dimensional digital representation of granular material microstructure from x-ray tomography imaging." *Journal of Computing in Civil Engineering*, 18(1), 28-35.

Wildenscheld, D., Hopmans, J. W., Vaz, C. M. P., Rivers, M. L., and Rikard, D. (2002). "Using X-ray computed tomography in hydrology: systems, resolutions, and limitations." *Journal of Hydrology*, 267(3-4), 285-297.

Wildenschild, D., Vaz, C. M. P., Rivers, M. L., Rikard, D., and Christensen, B. S. B. (2002). "Using X-ray computed tomography in hydrology: systems, resolutions, and limitations." *Journal of Hydrology*, 267(3–4), 285-297.

Yang, Q., and Kang, W. (2009). "General Research on Image Segmentation Algorithms " *International Journal of Image, Graphics and Signal Processing*, 1, 1-8.

Zelelew, H. M., and Papagiannakis, A. T. (2011). "A volumetrics thresholding algorithm for processing asphalt concrete X-ray CT images." *International Journal of Pavement Engineering*, 12(6), 543-551.